Applied Science and Engineering Progress, Vol. 20, No. 3, 2027, 8304

Research Article

Zinc Phosphate Coating Formation on Multi-Metal Materials: Effects of Bath pH and Temperature

Hisam Mansur, Irfan Purnawan and Athiek Sri Redjeki*
Department of Chemical Engineering, Universitas Muhammadiyah Jakarta, Jakarta, Indonesia

* Corresponding author. E-mail: athiek.sriredjeki@umj.ac.id DOI: 10.14416/j.asep.2026.09.005
Received: 14 May 2026; Revised: 7 July 2026; Accepted: 23 July 2026; Published online: 8 September 2026

Abstract
Multi-metal automotive bodies integrating steel and aluminum require adaptable zinc phosphate conversion coatings to provide corrosion protection. Zinc phosphate is widely applied prior to painting because it enhances both corrosion resistance and paint adhesion. However, comparative studies involving tri-cationic zinc phosphate on aluminum and steel remain limited. This study evaluated the effects of bath pH (2.4–3.6) and temperature (40–60 °C) on the coating performance of steel and aluminum substrates. Corrosion performance was assessed using a 72-hour salt spray test, combined with gravimetric weight-loss measurements, and supported by SEM–EDX characterization and adhesion testing. Zinc phosphate deposition on aluminum occurred at pH 3.3–3.6, forming plate-like crystals with incomplete surface coverage, whereas steel exhibited dense and uniform crystal structures at pH 3.0–3.3. Bath pH mainly influenced crystal nucleation and morphology, while higher temperatures promoted coating formation. The lowest corrosion rate for aluminum was 0.084 mm/year at pH 3.6 and 60 °C, whereas steel showed the lowest corrosion rate of 0.27 mm/year at pH 3.0 and 60 °C. Under these conditions, inhibition efficiencies reached 20.78% for aluminum and 84.49% for steel relative to the uncoated substrates. All coated samples achieved grade 5B adhesion in the tape test. The different optimum conditions observed for steel and aluminum highlight the challenge of using a single phosphating bath for multi-material automotive bodies.

Keywords: Conversion coating, Corrosion resistance, Multi metal pretreatment, Zinc phosphate

1 Introduction

Aluminum has been increasingly used since the second half of the twentieth century because of its lightweight characteristics, which contribute to vehicle weight reduction and lower carbon emissions [1], [2]. Automotive manufacturers such as Land Rover, Dyna-Panhard, and Audi have adopted aluminum and aluminum alloys for components including engine hoods, hardtops, and tailgates [3]. Nevertheless, steel remains the dominant structural material in automotive body construction owing to its favorable mechanical properties and cost-effectiveness [4]. Consequently, contemporary automotive architectures increasingly utilize a hybrid combination of ferrous and non-ferrous alloys, which undergo complex manufacturing sequences including advanced forming, dissimilar material joining, and surface conditioning [5]. The integration of heterogeneous metallic substrates within a single body structure requires effective pretreatment technologies capable of ensuring uniform corrosion mitigation and optimal coating adhesion across different material interfaces [6]. Among the available pretreatment technologies, zinc phosphate conversion coatings (ZPCCs) are widely employed prior to painting because they improve corrosion resistance and enhance paint adhesion [7]. These coatings form through reactions between the metal substrate and a phosphating bath containing phosphoric acid, metal ions, accelerators, and other additives, resulting in a thin, insoluble phosphate layer on the metal surface [8], [9].

Tri-cationic phosphating systems (Zn^{2+}, Ni^{2+}, and Mn^{2+}) are widely employed in automotive pretreatment processes because they provide superior crystal refinement, coating uniformity, and interfacial adhesion compared with conventional formulations [10]. In addition to chemical additives [11]-[14], the protective efficacy of these coatings is strongly

governed by operational parameters, particularly bath pH and temperature, which regulate substrate dissolution and crystal nucleation kinetics [15]. Recent studies have further demonstrated that these parameters significantly influence crystal morphology and deposition mechanisms. Alinezhadhfar *et al.,* [16] showed that variations in pH and temperature alter phosphate crystal growth and coating coverage on iron-based substrates, whereas Baloyi *et al.,* [17] reported distinct nucleation and growth behaviors between galvanized steel and aluminum alloys due to differences in substrate chemistry.

Despite these insights, the coupled effects of bath pH and temperature on steel and aluminum substrates under identical tri-cationic phosphating conditions remain insufficiently understood. This knowledge gap is particularly critical in modern automotive manufacturing lines, where heterogeneous metallic substrates are processed simultaneously and are expected to exhibit uniform coating quality and corrosion resistance [18]. Therefore, the present study systematically investigates the combined influence of bath pH and temperature on zinc phosphate coating formation and performance on both steel and aluminum substrates within a tri-cationic system. By comprehensively evaluating coating morphology, elemental composition, adhesion, and corrosion behavior, this work provides insight into the relationship between processing parameters and substrate type, thereby offering strategies for optimizing multi-metal pretreatment processes in automotive applications.

2 Materials and Methods

2.1 *Materials*

The substrates tested were aluminum and steel specimens measuring 70 × 150 × 0.8 mm. The aluminum substrate contained 10.92 wt.% C, 1.48 wt.% O, 0.62 wt.% Fe, and 86.97 wt.% Al, while the steel substrate contained approximately 13.73 wt.% C, 0.34 wt.% Al, and 85.93 wt.% Fe. All pretreatment solutions used before the zinc phosphate process were of commercial grade.

Commercial alkaline degreasing and activation products were employed according to the manufacturers' technical data sheets. Owing to proprietary restrictions, the product identities are not disclosed; however, their principal active components are summarized in Table 1. The tri-cationic zinc phosphate bath was formulated using 85% phosphoric acid (Shandong Near Chemical), 68% nitric acid (Qingdao Hisea Chem), zinc oxide (Indoxide), nickel carbonate (Hubei Tao Yuan Chemical), manganese carbonate (Shanghai Yuantai Chemical), sodium nitrite (Mudanjiang Fengda Chemicals), sodium nitrate (Hailan Chemical), and sodium fluoride (Shandong Pulisi Chemical).

Table 1: Composition of commercial pretreatment chemicals used before Zinc phosphating.

Stage	Component	Composition (mass %)
Degreasing	Sodium hydroxide	35-40
	Sodium carbonate	30-35
	Disodium metasilicate	15-20
Activation	Trizinc bis-orthophosphate	25-30

2.2 *Preparation of Pretreatment Baths*

The surface pretreatment process consisted of sequential degreasing, surface activation, tri-cationic zinc phosphating, and drying. The compositions of the degreasing, activator, and zinc phosphate baths are presented in Table 2. The zinc phosphate bath composition was formulated based on previously reported tri-cationic phosphating systems [19], [20]. Each degreasing solution, activator, and zinc phosphate bath was prepared in a 2000 mL glass beaker using deionized water, followed by the addition of raw materials according to the target composition. Each solution was mixed using a magnetic stirrer at 400 rpm.

Table 2: Composition of pretreatment bath solutions.

Stage	Component	Quantity
Degreasing	Degreasing product	1.65 wt.%
Activation	Activator product	0.2 wt.%
Phosphating	Phosphoric acid	13 g/L
	Nitric acid	2.84 g/L
	Zinc oxide	1.5 g/L
	Nickel carbonate	4 g/L
	Manganese carbonate	1.6 g/L
	Sodium nitrite	0.18 g/L
	Sodium nitrate	0.8 g/L
	Sodium fluoride	1.2 g/L

2.3 *Coating process*

Prior to pretreatment, the substrates were manually wiped using a clean, lint-free cloth to remove visible surface contaminants and dust. The specimens were then immersed in an alkaline degreasing solution at 40 °C for 120 s and rinsed with industrial water.

Afterward, the substrates were immersed in the activator bath for 30 s and immediately transferred to the zinc phosphate bath without intermediate rinsing. The phosphating process was conducted for 120 s using five pH levels (2.4, 2.7, 3.0, 3.3, and 3.6) and five temperature levels (40, 45, 50, 55, and 60 °C), resulting in 25 experimental conditions based on a full factorial design. The selected pH and temperature ranges were established based on previous studies of zinc phosphate and tri-cationic phosphating systems [16], [17], [19].

A fresh phosphating bath was prepared for each pH–temperature combination to eliminate the influence of bath aging. For each condition, three steel specimens and three aluminum specimens were sequentially processed using the same bath. Among the coated specimens, two panels of each substrate were used for corrosion testing, while the remaining panel was subsequently coated with cathodic electrodeposition (CED) epoxy paint and used for adhesion evaluation.

During phosphating, continuous agitation was maintained using a magnetic stirrer operating at 400 rpm to ensure bath homogeneity. The bath pH was measured using a Horiba LAQUA 200 series pH meter immediately after bath preparation and was adjusted with phosphoric acid or 1 M NaOH to achieve the target values. After phosphating, the specimens were rinsed by spraying with demineralized water for 30 s and then dried in an oven at 80 °C for 10 min. The CED process was conducted at a bath temperature of 30 °C, with an immersion time of 3 min and an applied voltage of 200 V, producing an epoxy coating with a dry-film thickness of 17 ± 1 µm. The coated specimens were subsequently cured at 105 °C for 2 h. A schematic illustration of the coating process is shown in Figure 1.

2.4 *Characterization and performance testing*

2.4.1. Characterization

The surface morphology of the zinc phosphate coatings was characterized using a scanning electron microscope (SEM, JEOL IT2100) equipped with an energy-dispersive X-ray spectroscopy (EDX) detector for elemental analysis. SEM observations were conducted at a magnification of 1500× with an accelerating voltage of 15 kV. Elemental composition was determined from a representative point on the coating surface using EDX analysis. No conductive coating was applied prior to SEM examination.

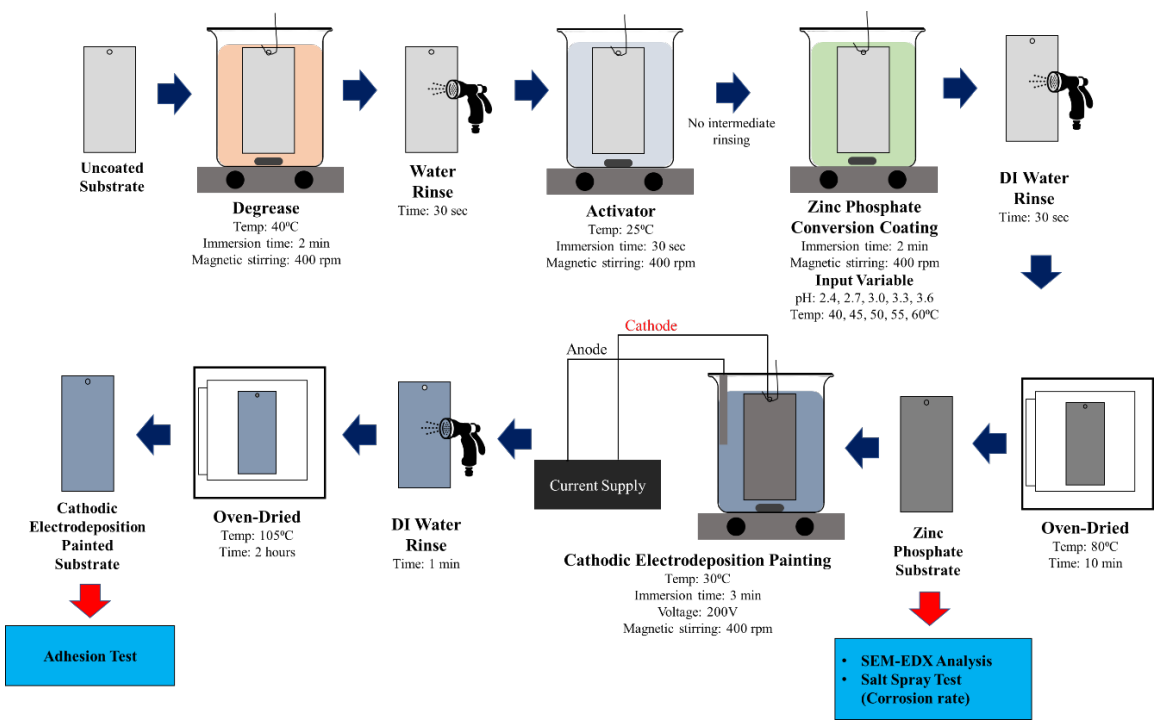

Figure 1: Schematic illustration of the coating process.

Applied Science and Engineering Progress, Vol. 20, No. 3, 2027, 8304

2.4.2. Corrosion rate performance

The corrosion resistance of the phosphate-coated substrates was evaluated using a salt spray test in accordance with ASTM B117. Corrosion testing was performed on phosphate-coated specimens without additional paint layers. For each experimental condition, two specimens of each substrate were exposed in a salt spray chamber containing 5 wt.% NaCl solution at 35 °C for 72 h. After exposure, corrosion products were removed following ASTM G1-03. Aluminum specimens were cleaned using nitric acid, whereas steel specimens were cleaned using hydrochloric acid containing hexamethylenetetramine. The cleaned specimens were subsequently weighed to determine weight loss, and the corrosion rate was calculated using Eq. (1).

$$V_{corr} = \frac{K \times W}{A \times t \times D} \left(^{mm}/_{year}\right) \quad (1)$$

where K is the corrosion rate constant (87.6), W is the average weight loss (mg), A is the exposed area (210 cm^2), t is the exposure time (h), and D is the substrate density (2.69 g/cm^3 for aluminum and 7.85 g/cm^3 for steel). The inhibition efficiency (IE%) of the substrates was calculated using Eq. (2), where W_0 is the weight loss of the control sample (uncoated substrate) and W is the weight loss of the ZPCC substrate. All experiments were conducted in duplicate, and average values are reported. Standard deviations were used to evaluate data variability, while error bars were omitted to improve figure readability.

$$IE\ \% = \frac{W_0 - W}{W_0} \quad (2)$$

2.4.3. Adhesion Performance

Adhesion performance was evaluated on zinc phosphate-coated substrates that were subsequently coated with commercial epoxy-based CED paint. For each experimental condition, one specimen of each substrate was subjected to a cross-hatch adhesion test in accordance with ASTM D3359 (Method B). A cutting guide (Taiyu Kizai No. 315) with a blade spacing of 1 mm and a utility knife (Joyko A-300A) were used to produce eleven parallel cuts, followed by a second set of perpendicular cuts to form a lattice pattern. Adhesive tape (NICHIBAN Cellotape CT/No. 405) was then applied to the grid and removed according to the ASTM D3359 procedure. Adhesion performance was evaluated qualitatively and classified from 5B to 0B.

3 Results and Discussion

3.1 *Morphological characterization*

3.1.1. SEM micrographs of aluminum

The surface morphology of the zinc phosphate layer was characterized using SEM. Figure 2(a)–(e) shows the surface morphology of the zinc phosphate layer formed on the aluminum substrate at various pH values. Crystal formation was observed only at pH 3.3 and 3.6, with flat and fine crystal morphology. Although crystals were present under both conditions, the resulting layer did not completely cover the surface, and some areas of the aluminum remained exposed. Upon closer observation, cracks were detected on the aluminum surface under conditions where no crystal layer was formed.

The presence of cracks under non-crystal-forming conditions suggests that the phosphate crystal formation reaction was suppressed, whereas cracking still occurred because of hydrogen evolution and dehydration during the coating process [21]. The incomplete crystal layer indicates that the aluminum surface was not fully protected. The presence of uncovered regions may allow electrolytes to penetrate the layer, thereby increasing the possibility of corrosion initiation [22]. To maximize crystal coverage, the immersion duration may be extended, or the process temperature may be increased [17].

Figure 3(a)–(e) shows that higher temperatures increased the degree of surface coverage, resulting in fewer uncovered gaps. However, even at the highest temperature used in this study, gaps between crystals were still observed. The reduction in uncovered regions indicates that increasing the temperature of the zinc phosphate bath promotes crystal growth by accelerating the coating reaction and facilitating crystal deposition [23].

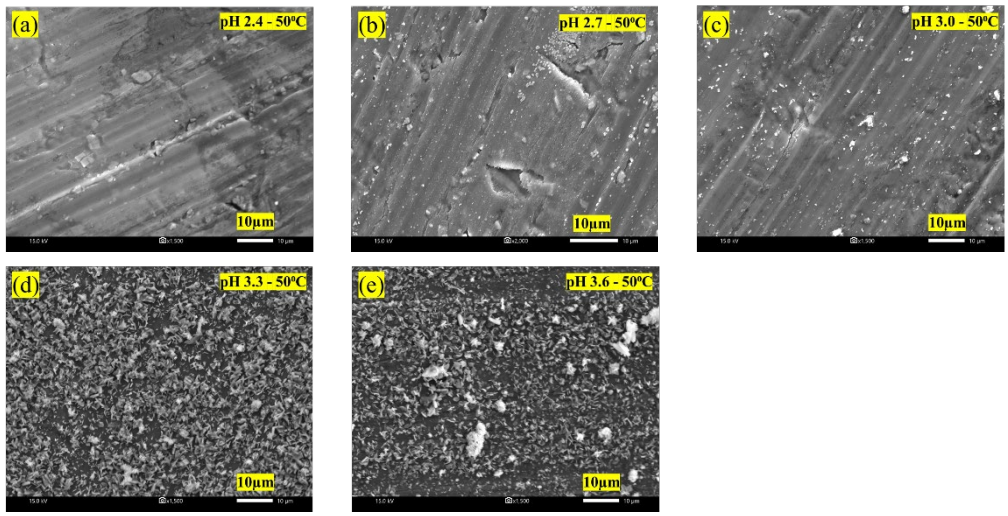

Figure 2: SEM micrographs of Zinc phosphate conversion coatings on aluminum at various pH values.

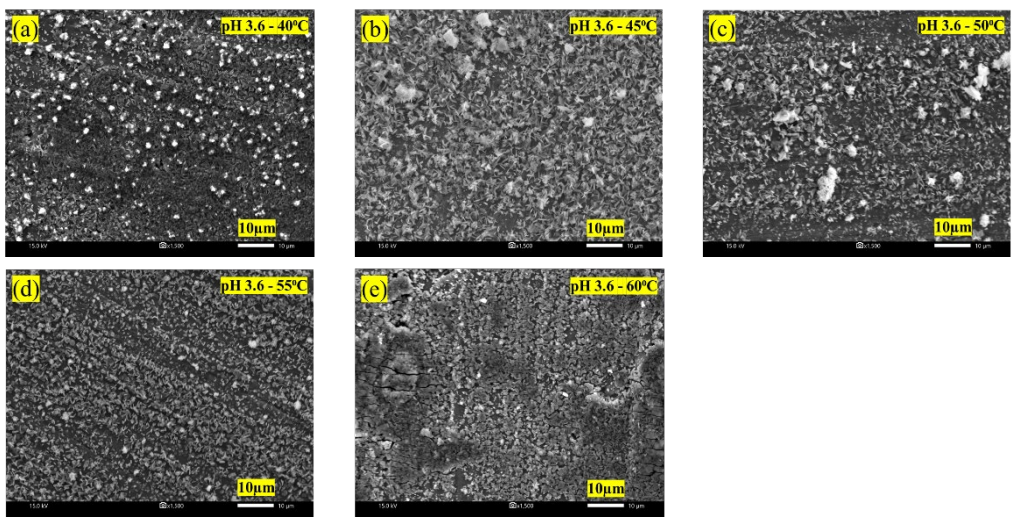

Figure 3: SEM micrographs of zinc phosphate conversion coatings on aluminum at various temperatures.

Baloyi *et al.,* [17] reported that higher operating temperatures resulted in lower corrosion current density, indicating a reduced corrosion rate. Based on the results of the present study, crystal deposition may be maximized by prolonging the immersion duration in the zinc phosphate bath [24]. Additionally, previous studies have shown that increasing the sodium fluoride concentration can improve crystal deposition, with the optimum range reported as 1.2–1.4 g/L [20]. Overall, zinc phosphate coating on aluminum was obtained only at pH 3.3 and 3.6. Although increasing the temperature improved surface coverage, complete crystal coverage was not achieved under the conditions investigated in this study.

3.1.2. SEM micrographs of steel

Figure 4(a)–(e) shows that the zinc phosphate layer formed on the steel surface completely covered the substrate, with no uncovered voids observed. Differences in crystal morphology were observed at each pH level. At pH 2.4, the crystals exhibited a long needle-like morphology with sharp tips. At pH 2.7 and 3.0, the crystals became shorter, with more oval

Applied Science and Engineering Progress, Vol. 20, No. 3, 2027, 8304

terminations. In contrast, at pH 3.3 and 3.6, the crystals were rounder, denser, and more uniform.

The variation in crystal morphology indicates that pH has a significant effect on crystal deposition on the steel surface. The main processes occurring when a substrate is immersed in a zinc phosphate bath are Fe dissolution and continuous crystal layer formation [24]. At lower pH levels, the addition of phosphoric acid promotes more aggressive dissolution of iron ions [25]. Under these acidic conditions, dissolution is dominant; once crystal nuclei begin to form, they grow larger and develop a more elongated morphology [16].

However, as pH increases, dissolution becomes less aggressive. Consequently, once crystal nuclei are formed, their growth becomes slower, producing more rounded and uniform crystals [26]. These rounded, dense, and uniform layers are associated with improved corrosion resistance [27]. Previous studies have reported that the optimum pH range for obtaining uniform crystal morphology on steel is 2.9–3.1, which is generally consistent with the results of this study [19], [28].

The effect of temperature on zinc phosphate formation was also investigated to determine its influence on morphology, as shown in Figure 5(a)–(e). At 40 °C, the crystals appeared as short spherical

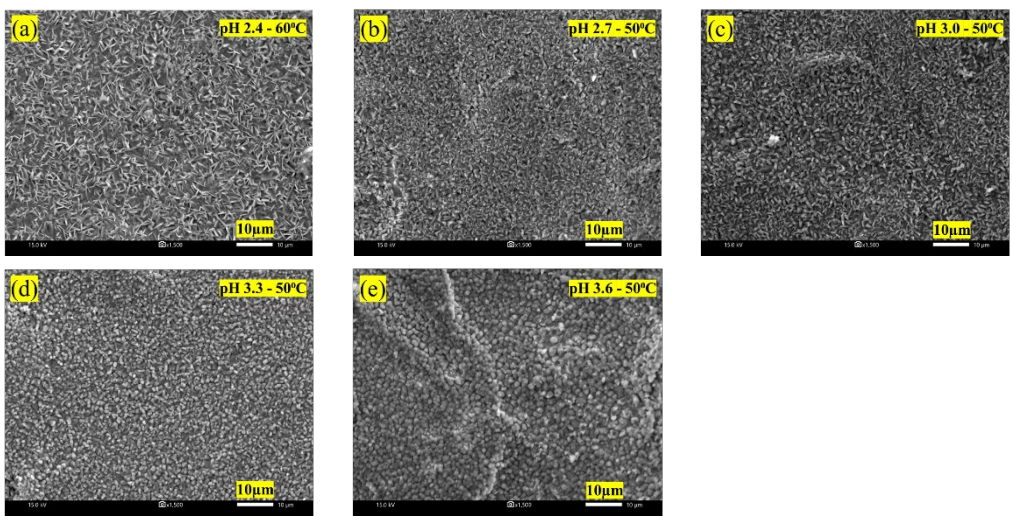

Figure 4: SEM micrographs of Zinc phosphate conversion coatings on steel at various pH values.

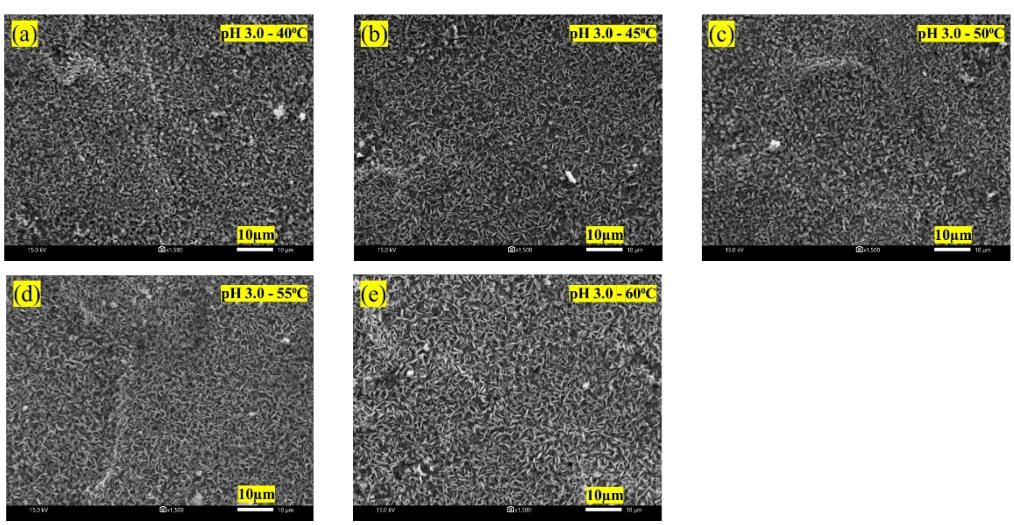

Figure 5: SEM micrographs of Zinc phosphate conversion coatings on steel at various temperatures.

structures stacked on top of one another, with visible gaps between adjacent crystals. As the temperature increased, the crystals grew larger and gradually developed into flattened needle-like structures. This indicates that temperature plays a role in promoting more aggressive crystal formation. Díaz *et al.,* [15] reported similar behavior, showing that increasing temperature resulted in a significant decrease in the current measured using an electrochemical cell, indicating a more active layer formation process. Furthermore, increasing temperature can enhance both the weight and thickness of the zinc phosphate layer [29]. Based on these results, pH influences crystal morphology, while temperature increases the rate of crystal formation.

3.2 *EDX Elemental composition*

3.2.1. Elemental composition of ZPCC on aluminum

Several elements were detected on the aluminum substrate, including carbon (C), aluminum (Al), oxygen (O), phosphorus (P), and zinc (Zn), together with small amounts of manganese (Mn), nickel (Ni), iron (Fe), and fluorine (F). As shown in Figure 6, phosphorus was detected only at pH 3.3 and 3.6, indicating that zinc phosphate deposition occurred only under these conditions. The highest phosphorus content was obtained at pH 3.3 and 60 °C, reaching 11.26 wt.%, with an aluminum content of 24.8 wt.%. The simultaneous presence of Zn and P is consistent with the formation of zinc phosphate compounds, which are commonly reported on aluminum substrates [20]. Aluminum signals were still detected even under conditions where phosphorus was present. This observation suggests that the substrate was not completely masked by the deposited layer, which is consistent with the incomplete surface coverage observed in the SEM images [30].

3.2.2. Elemental composition of ZPCC on steel

Based on the EDX analysis results, several elements were detected on the steel substrate layer, including carbon (C), oxygen (O), phosphorus (P), iron (Fe), manganese (Mn), nickel (Ni), and zinc (Zn). Figure 7(a) shows the presence of phosphorus (P), indicating the successful formation of a zinc phosphate crystal layer. The phosphorus content generally increased with increasing pH up to 3.3, followed by a decrease at pH 3.6, as shown in Figure 7. The highest phosphorus content was obtained at pH 3.3 and 60 °C, reaching 9.64 wt.%, whereas the lowest value was observed at pH 2.4 and 40 °C, with a phosphorus content of 0.45 wt.%. These results indicate that the amount of deposited phosphate species depends on the bath conditions and suggest the existence of an optimum pH range for obtaining a layer with relatively high phosphorus content. The decrease in phosphorus content at pH 3.6 implies that excessively high pH may reduce the efficiency of phosphate deposition.

Iron was also detected in the EDX spectra, which may be attributed to iron dissolution during the phosphating process, followed by its incorporation into zinc phosphate compounds [7]. The simultaneous presence of P and Fe suggests the formation of mixed zinc phosphate compounds commonly reported on steel substrates. SEM–EDX analysis provides only elemental composition and distribution, making the identification

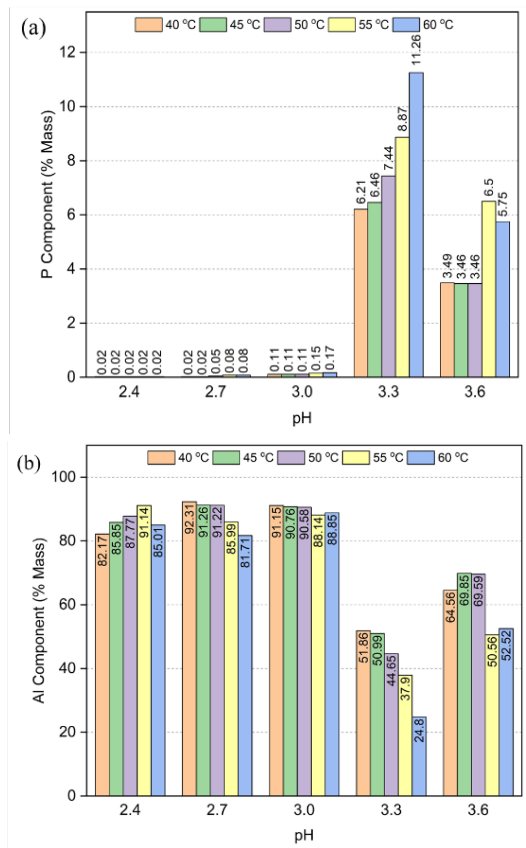

Figure 6: Elemental composition of ZPCC on the Aluminum substrate: (a) P content and (b) Al content.

Applied Science and Engineering Progress, Vol. 20, No. 3, 2027, 8304

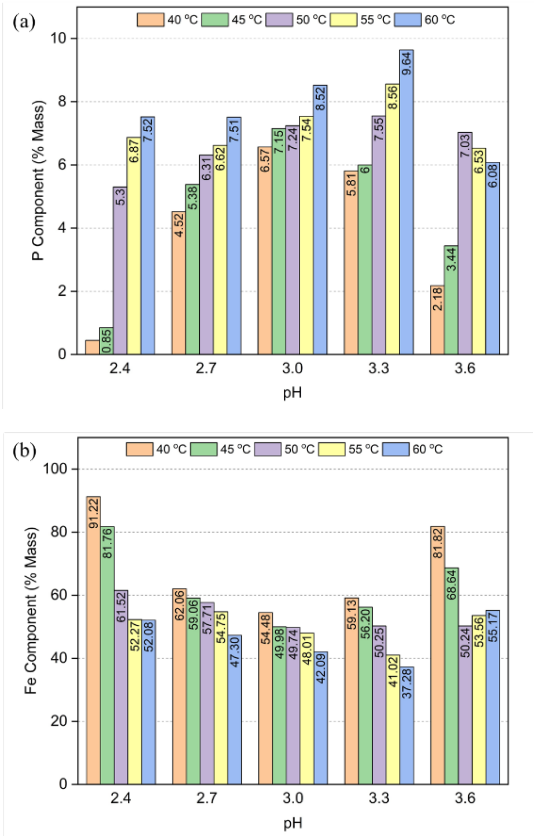

Figure 7: Elemental composition of ZPCC on the steel substrate: (a) P content and (b) Fe content.

of specific zinc phosphate phases tentative. Definitive phase identification requires complementary techniques such as X-ray diffraction (XRD) [31]. Additionally, SEM–EDX alone is insufficient for the quantitative measurement of coating thickness and porosity.

3.3 *Corrosion rate*

3.3.1. Corrosion rate of aluminum

Corrosion rates were evaluated by measuring weight loss using gravimetric analysis after a 72-hour salt spray test (SST). Inhibition efficiency (IE) values were calculated by comparing the weight loss of the coated samples with that of the uncoated control sample. Based on these data, the corrosion rate and inhibition efficiency of the coating were determined, allowing further interpretation of coating degradation behavior. The average weight loss of the uncoated substrate after testing was 43.2 mg, and inhibition efficiency was calculated using Eq. (2). Figure 8(a) presents the weight loss of aluminum substrates treated with ZPCC. At pH values between 2.4 and 3.0, the weight loss values were relatively similar to those of the control sample and, in some cases, were even higher. These results indicate that the phosphating treatment did not provide effective corrosion protection because a zinc phosphate layer had not formed on the aluminum surface. In contrast, lower weight loss values were observed at pH 3.3 and 3.6 compared with the control sample.

The corrosion rate of aluminum under various ZPCC bath conditions is shown in Figure 8(b). In general, relatively high corrosion rates were observed at low pH values, between 2.4 and 3.0. In agreement with the SEM–EDX results, these conditions corresponded to the absence of zinc phosphate layer formation. A reduction in corrosion rate was observed at pH 3.3 and 3.6, coinciding with the formation of a zinc phosphate layer. The lowest corrosion rate was obtained at pH 3.6 and 60 °C, with a value of 0.084 mm/year. Although the optimum phosphating bath temperature in this study was 60 °C, which may lead to higher energy consumption, this temperature remains within the typical operating range of 40–90 °C reported in the literature [15], [16], [32], [33].

Figure 8(c) shows that the inhibition efficiency of the coated substrates increased with increasing phosphating bath temperature, indicating improved corrosion protection. This observation is consistent with the SEM–EDX results, which confirmed the presence of zinc phosphate deposition on the aluminum surface at pH 3.3–3.6. However, the relatively small difference in weight loss between the coated and uncoated substrates may be attributed to the naturally occurring protective oxide layer (Al_2O_3) on the aluminum surface, which already provides a certain degree of corrosion resistance [34]. Among all conditions, the highest inhibition efficiency was achieved at pH 3.6 and 60 °C, reaching 20.78%.

Representative appearances of the aluminum substrate before coating, after coating, and after the SST are presented in Figure 9(a)–(c). As shown in Figure 9(c), the surface became rougher and exhibited a yellowish appearance after the SST. The corrosion process begins with the dissolution of the Al_2O_3 layer commonly present on the aluminum surface [35]. Chloride ions originating from the salt solution used in the test promote pitting corrosion of aluminum [36].

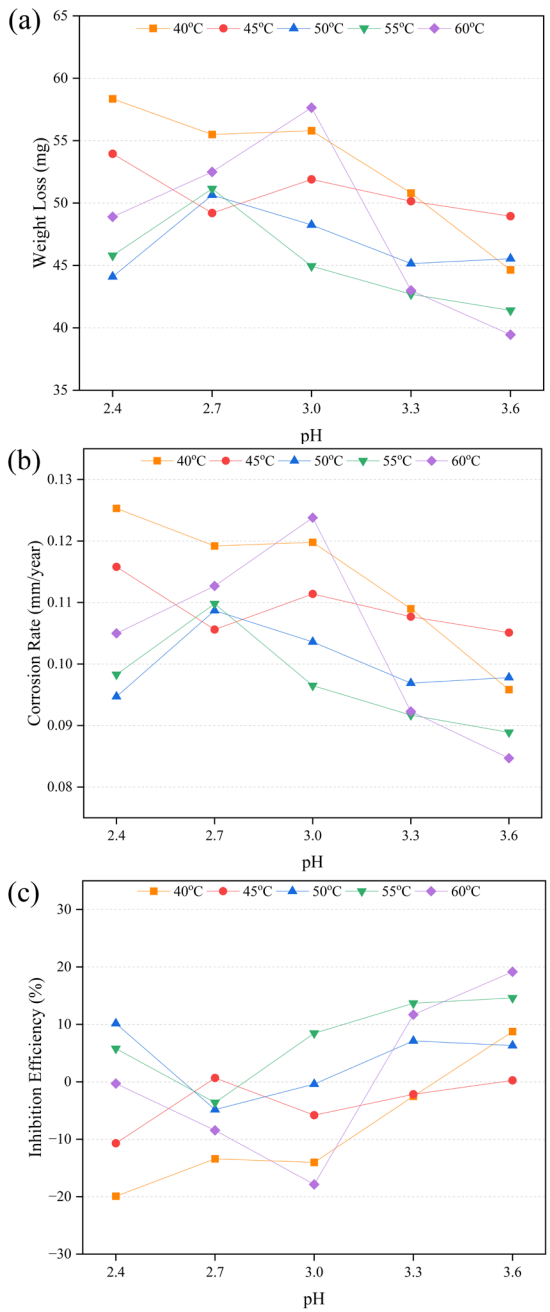

Figure 8: ZPCC on aluminum after a 72-hour salt spray test: (a) weight loss, (b) corrosion rate, and (c) inhibition efficiency. Data are presented as mean values (n = 2).

Under atmospheric corrosion conditions with constant temperature and humidity, corrosion products formed on the aluminum surface generally consist of $Al(OH)_3$, AlO(OH), Al_2O_3, and $AlCl_3$ [37].

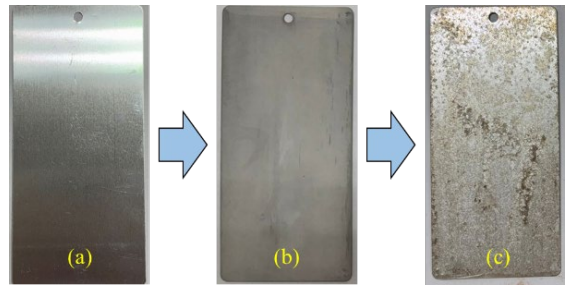

Figure 9: Representative appearance of the aluminum substrate: (a) uncoated, (b) after ZPCC, and (c) after the salt spray test.

3.3.2. Corrosion rate of steel

As shown in Figure 10(a), the weight loss measurements indicated that the greatest material loss occurred under highly acidic conditions, with a maximum value of 1.69×10^3 mg recorded at pH 2.4 and 40 °C. However, this value was still lower than that of the uncoated steel substrate, which exhibited an average weight loss of 2.42×10^3 mg. At the same pH, increasing the zinc phosphate bath temperature resulted in lower weight loss, indicating that higher bath temperatures improved corrosion protection.

The corrosion rates under different bath conditions are presented in Figure 10(b). Both bath pH and temperature significantly affected the corrosion rate of the coated steel. The highest corrosion rate, with a value of 1.24 mm/year, was observed at pH 2.4 and 40 °C. This condition corresponded to the lowest phosphorus content detected by EDX analysis. In general, the corrosion rate decreased with increasing bath temperature across all pH conditions. However, a different trend was observed at pH 3.6, where the corrosion rate began to increase. This result suggests that optimum coating performance is achieved within a limited pH range [16]. The lowest corrosion rate was achieved at pH 3.0 and 60 °C, with a value of 0.27 mm/year and an inhibition efficiency of 84.5%. Under these conditions, the EDX results showed a relatively high phosphorus content of 8.52 wt.%. Although the highest phosphorus content was observed at pH 3.3 and 60 °C, it did not correspond to the optimum corrosion protection.

SEM observations indicate that crystal morphology also plays an important role in corrosion resistance. At pH 3.0, finer and smaller crystals were observed. Similar observations were reported by Ramos *et al.,* [24], who showed that smaller and more compact phosphate crystals provide better corrosion

resistance than larger crystals because of reduced intercrystalline gaps. Therefore, the combination of high phosphorus deposition and fine, compact crystals contributed to the lowest corrosion rate.

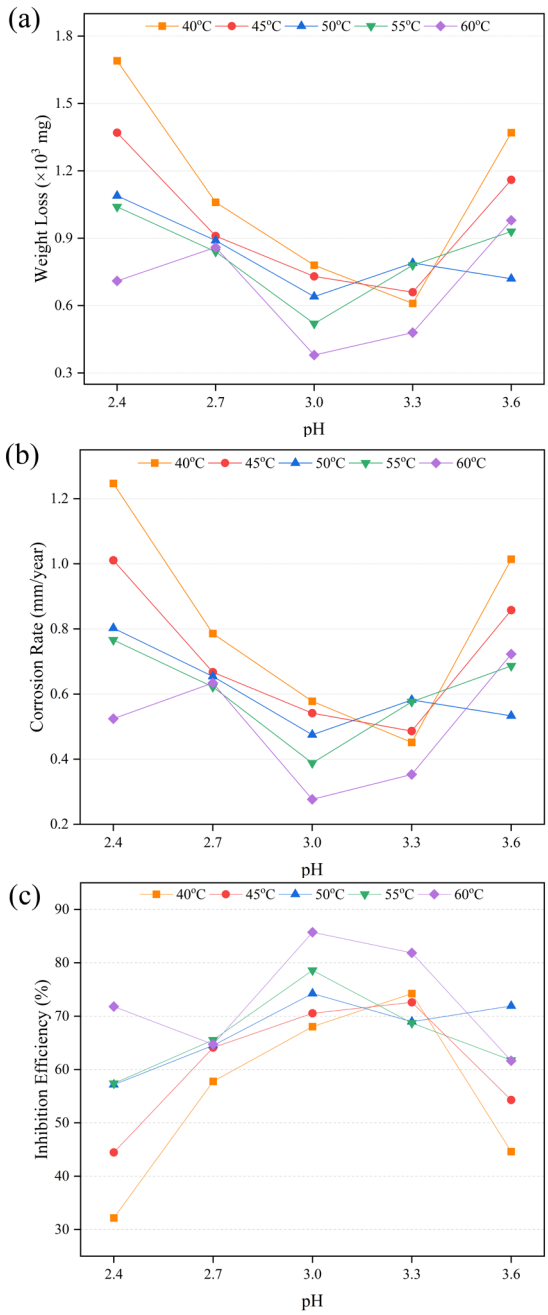

Figure 10: ZPCC on steel after a 72-hour salt spray test: (a) weight loss, (b) corrosion rate, and (c) inhibition efficiency. Data are presented as mean values (n = 2).

Representative appearances of the steel substrate before coating, after coating, and after the SST are presented in Figure 11(a)–(c). Similar to aluminum, the corrosion process began with substrate dissolution, resulting in a high concentration of dissolved Fe ions near the metal surface [38]. Subsequently, the Fe ions reacted with phosphate species to form iron phosphate precipitates as corrosion products [39].

3.4 *Adhesion*

Aluminum and steel substrates coated with zinc phosphate were further coated with epoxy resin paint via CED. Adhesion testing was conducted using the lattice pattern method with eleven cuts in each direction, followed by the application and removal of pressure-sensitive tape over the lattice. Figure 12 presents the adhesion test results of the CED-coated substrates. Based on the ASTM D3359 classification, all samples achieved a 5B rating, indicating zero paint loss from the specimens. Because all tested conditions yielded identical maximum adhesion ratings, the influence of zinc phosphate bath variations on adhesion performance could not be clearly distinguished using this method.

Figure 11: Representative appearance of the steel substrate: (a) uncoated, (b) after ZPCC, and (c) after the salt spray test.

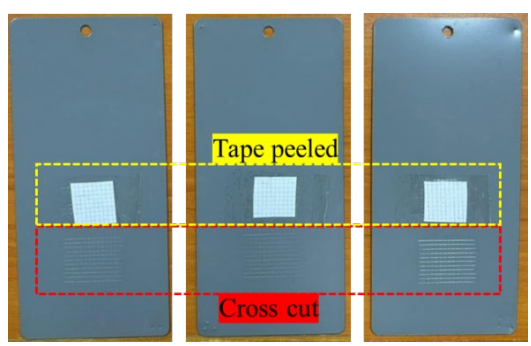

Figure 12: Representative adhesion test result on the painted substrate.

The uniformly high adhesion observed may be associated with the inherently strong bonding characteristics of CED coatings, which possess high surface functionality through peripheral hydroxyl groups and ether bonds [40]. Although a porous zinc phosphate structure is generally considered important for promoting mechanical interlocking between the metal surface and the paint layer, the high adhesion capability of the CED system and the surface preparation procedures employed in this study may have limited the ability of the ASTM D3359 test to detect subtle differences in adhesion performance [41], [42].

This behavior was also observed for aluminum substrates processed under bath conditions below pH 3.3. Despite limited zinc phosphate deposition under these conditions, all samples still exhibited excellent adhesion. This result may be attributed to the NaOH-based degreasing process, which effectively removes oils and surface contaminants [43], thereby providing sufficient surface cleanliness before coating application [44].

3.5 *Zinc Phosphate Coating Mechanism*

Based on mechanisms proposed in previous studies, zinc phosphate coating formation on aluminum generally involves substrate dissolution, crystal nucleation, and dynamic equilibrium between coating growth and dissolution [3], [45], as schematically illustrated in Figure 13. The reactions presented in this section are intended to provide a mechanistic framework for interpreting the experimental observations and do not constitute direct evidence obtained in the present study. The first stage involves dissolution of the substrate by hydrogen derived from phosphoric acid. Oxidation occurs at the anode, and hydrogen is formed at the cathode through the following reactions.

$$Al_2O_3 + 6H^+ \rightarrow 2Al^{3+} + 3H_2O \quad (3)$$

$$Al + 3H^+ \rightarrow Al^{3+} + 1\,{}^1\!/_2\, H_{2(g)} \quad (4)$$

The increase in pH near the aluminum surface shifts the equilibrium of phosphoric acid, resulting in the production of more phosphate ions, which in turn triggers the formation and growth of the coating layer.

A more complex reaction pathway occurs on aluminum substrates because fluoride ions interact with dissolved aluminum species. Fluoride ions are commonly added to promote coating formation by removing the passive oxide layer; however, excessive complexation between Al^{3+} and F^- may reduce the availability of aluminum ions near the interface and influence the coating process [3].

$$Al^{3+} + 6F^- \rightarrow AlF_6^{3-} \quad (5)$$

The next step is crystal formation, as illustrated by the following reaction. When the solution becomes saturated with PO_4^{3-} and Zn^{2+}, and the pH rises near the substrate surface, insoluble phosphate precipitates and crystallizes on the substrate layer, forming the conversion coating.

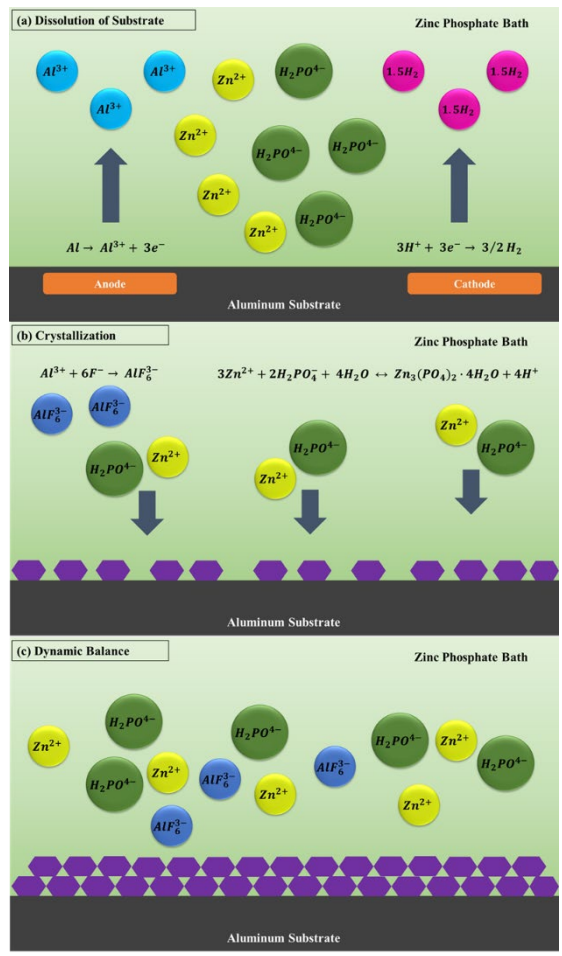

Figure 13: Schematic representation of the proposed zinc phosphate coating mechanism on aluminum, derived from the literature.

Applied Science and Engineering Progress, Vol. 20, No. 3, 2027, 8304

$$3Zn^{2+} + 2H_2PO_4^- + 4H_2O \leftrightarrow Zn_3(PO_4)_2 \cdot 4H_2O + 4H^+ \text{ (Hopeite)} \quad (6)$$

Under the equilibrium conditions described above, the system can be disrupted by changes in bath conditions, such as pH, temperature, or solution concentration [16]. In the present study, the cracks observed at pH 2.4–3.0 (Figure 2(a)–(c)) are consistent with conditions in which substrate dissolution predominates over crystal growth. However, the occurrence of these reactions was not directly verified and is inferred from surface morphology together with mechanisms reported in the literature.

The final stage of the conversion coating process involves a balance between crystal growth and dissolution. During coating formation, local pH changes near the surface cause dissolution and layer formation to occur simultaneously [26]. Initially, the process is dominated by layer growth; gradually, the rates of both processes converge, although dissolution eventually becomes more dominant [46].

During phosphating, phosphate sludge is inevitably formed. Sludge accumulation can reduce bath stability and coating consistency [45]. Therefore, industrial phosphating baths are commonly equipped with continuous circulation and filter press systems [47]. The generated wastewater typically requires a combination of physicochemical and biological treatment processes before safe discharge or industrial reuse [48].

$$Al^{3+} + 6F^- + 3Na^+ \rightarrow Na_3AlF_6 \quad (7)$$

$$Al^{3+} + 6F^- + 2K^+ + 3Na^+ \rightarrow K_2NaAlF_6 \quad (8)$$

The coating process on steel substrates generally follows the same stages as those previously described for aluminum. The main difference lies in the dissolution stage, where iron (Fe) from the steel substrate dissolves to form Fe^{2+} ions [3]. No complexation reaction occurs on steel, unlike on the aluminum substrate. The reaction process on the steel substrate is described in the following reactions.

Dissolution:

$$Fe + 2H_3PO_4 \rightarrow Fe(H_2PO_4)_2 + H_{2(g)} \quad (9)$$

$$Fe + 2H^+ \rightarrow Fe^{2+} + H_{2(g)} \quad (10)$$

Coating formation:

$$3Zn^{2+} + 2H_2PO_4^- + 4H_2O \leftrightarrow Zn_3(PO_4)_2 \cdot 4H_2O + 4H^+ \text{ (Hopeite)} \quad (11)$$

$$2Zn^{2+} + Fe^{2+} + 2H_2PO_4^- + 4H_2O \leftrightarrow Zn_2Fe(PO_4)_2 \cdot 4H_2O + 4H^+ \text{ (Phosphophyllite)} \quad (12)$$

Sludge generation:

$$Fe^{3+} + H^+ + O_x \rightarrow Fe^{3+} + HO_x \quad (13)$$

$$Fe^{3+} + H_2PO_4^- \rightarrow FePO_4 2H^+ \quad (14)$$

4 Conclusion

This study highlights the practical challenges of using a single zinc phosphating bath for the simultaneous treatment of steel and aluminum substrates. Increasing temperature promoted coating formation, while pH mainly governed crystal nucleation and morphology. The best corrosion performance was obtained at 60 °C, with optimum pH values of 3.6 for aluminum and 3.0 for steel. The results show that the optimum phosphating conditions differed between the two materials, indicating that a compromise in bath parameters is required to achieve balanced coating performance on dissimilar metals. Therefore, an intermediate operating window may be necessary for multi-substrate automotive pretreatment processes. Although such conditions may not provide the optimum phosphate layer characteristics for each substrate individually, all CED-coated samples exhibited excellent adhesion. These findings suggest that the combined phosphating–CED process remains a practical approach for modern multi-material automotive bodies. Further studies are required to determine the optimum operating window for shared phosphating baths used for dissimilar metals.

Acknowledgments

This project received financial support from the Internal Research Grant of Universitas Muhammadiyah Jakarta, managed by the Center of Research, Development and Community Services under contract number 280/R-UMJ/XI/2025.

Author Contributions

H.M.: conceptualization, methodology, writing—original draft, visualization, field study, investigation, review, and editing. I.P.: investigation, data analysis, data curation, writing—review and editing. A.S.R.: conceptualization, data curation, writing—review and editing, funding acquisition, and corresponding author. All authors have read and agreed to the published version of the manuscript.

Conflicts of Interest

The authors declare that they have no known competing financial interests or personal relationships that could have appeared to influence the work reported in this paper.

Declaration of generative AI and AI-assisted technologies in the writing process

The authors used AI as a tool to improve the language, grammar, and readability of the manuscript. All generated outputs were carefully reviewed and edited by the authors, who take full responsibility for the content of the publication.

References

[1] S. S, V. S, K. P, and S. B. B, "Optimization of wear behaviour of Al6061 metal matrix composites using Taguchi approach," *Turkish Journal of Engineering*, vol. 9, no. 1, pp. 56–63, Jan. 2025, doi: 10.31127/tuje.1502413.

[2] S. Saifudin, N. Muhayat, E. Surojo, Y. H. Manurung, and T. Triyono, "Mitigation of porosity and residual stress on car body aluminum alloy vibration welding: A systematic literature review," *Automotive Experiences*, vol. 5, no. 3, pp. 477–493, Nov. 2022, doi: 10.31603/ae.7965.

[3] H. Streitberger and K. Dössel, Eds., *Automotive Paints and Coatings*, 1st ed. Weinheim, Germany: Wiley-VCH, 2008, doi: 10.1002/9783527622375.

[4] M. Heidari et al., "Circular economy pathways for decarbonizing aluminum and steel automotive body sheet components in the United States," *Resources, Conservation and Recycling*, vol. 226, Art. no. 108654, Feb. 2026, doi: 10.1016/j.resconrec.2025.108654.

[5] P. Shrivastava et al., "A comprehensive review on advanced materials and testing techniques for passenger vehicle frames," *Materials Today Communications*, vol. 54, Art. no. 115480, Jun. 2026, doi: 10.1016/j.mtcomm.2026.115480.

[6] U. Nirmal, M. A. Musa, M. Y. Yuhazri, and M. M. H. M. Ahmad, " Development of car coating materials over the past decade for paint protection applications—An overview on the different types of paint protections," *Polymers*, vol. 17, no. 23, Art. no. 3114, Nov. 2025, doi: 10.3390/polym17233114.

[7] S. A. Barsana, A. S. Nasar, and M. J. Umapathy, "Enhanced corrosion resistance of zinc phosphate coatings on mild steel through incorporation of nanocrystalline CeO2 and CeO2–CuO nanocomposite," *RSC Advances*, vol. 15, no. 26, pp. 20916–20934, Jun. 2025, doi: 10.1039/D5RA02800K.

[8] M. Alinezhadfar et al., "Wear mechanism of activated zinc phosphate conversion coatings under dry and lubricated sliding," *Applied Surface Science*, vol. 736, Art. no. 166722, Aug. 2026, doi: 10.1016/j.apsusc.2026.166722.

[9] L. Elias, C. V. Geethanjali, B. I. Bijimol, A. Anil, M. A. Shafna, and S. M. A. Shibli, "Influence of fine-recycled concrete aggregate derived SiO2 composite on corrosion protection and anti-wear characteristics of zinc and zinc phosphate coatings," *Journal of Industrial and Engineering Chemistry*, vol. 152, pp. 396–410, Dec. 2025, doi: 10.1016/j.jiec.2025.05.009.

[10] G. Khalaj, A. Najafi, and A. Heidarian, "Investigating and characterizing the effect of zinc-nickel-manganese cation concentration on the properties of phosphate coating of 41Cr4 steel," *Jicers*, vol. 19, no. 4, pp. 20–35, Mar. 2024.

[11] S. Korniy, M.-O. Danyliak, and S. Lavrys, "Preparation and properties of modified montmorillonite by zinc-phosphate for anticorrosion applications in protective coatings," *Materials Chemistry and Physics*, vol. 335, Art. no. 130537, Apr. 2025, doi: 10.1016/j.matchemphys.2025.130537.

[12] X. Zhang, H.-H. Zhang, K. Wu, Y. Zhang, Z.-N. Yang, and Y. Chen, "Effect of calcium nitrate on microstructure and anti-corrosion properties of zinc phosphate coatings on stainless steel,"

Coatings, vol. 15, no. 9, Art. no. 1018, Sep. 2025, doi: 10.3390/coatings15091018.

[13] Q. Ma et al., "Trivalent cerium-doped zinc phosphate composite coating: A novel solution to the wear-corrosion coupling issue," *Surface and Coatings Technology*, vol. 509, Art. no. 132213, Aug. 2025, doi: 10.1016/j.surfcoat.2025.132213.

[14] K. Tang et al., "Micromorphology evolution and properties of strontium-zinc-phosphate chemical conversion coatings on Ti: Effect of Zn2+ and Ca2+ in the reaction solution," *Surfaces and Interfaces*, vol. 56, Art. no. 105504, Jan. 2025, doi: 10.1016/j.surfin.2024.105504.

[15] B. Díaz, I. Feijoo, X. R. Nóvoa, C. Pérez, A. Pintos, and S. Silva-Fernández, "Preparation and characterization of phosphate coatings developed on 316 L by a cathodic treatment," *Electrochimica Acta*, vol. 525, Art. no. 146093, Jun. 2025, doi: 10.1016/j.electacta.2025.146093.

[16] M. Alinezhadfar, P. Schmutz, F. E. Furcas, J. Reuteler, R. Crockett, and U. Angst, "Mechanism of zinc phosphate conversion coating formation on iron-based substrates," *Corrosion Science*, vol. 248, Art. no. 112796, May 2025, doi: 10.1016/j.corsci.2025.112796.

[17] T. Baloyi, N. Maledi, and A. Andrews, "Corrosion performance of zinc phosphate coatings deposited on AA6061-HDG steel," *Materials Chemistry and Physics*, vol. 283, Art. no. 126009, May 2022, doi: 10.1016/j.matchemphys.2022.126009.

[18] C. F. Glover et al., "A comparative study of zinc phosphate and zirconium-based conversion coatings on galvannealed steel: Effect on corrosion performance of electrocoated systems," *Corrosion*, vol. 80, no. 7, pp. 755-769, Jul. 2024, doi: 10.5006/4108.

[19] A. Heydarian, A. Najafi, and G. Khalaj, "Enhancement of low-zinc phosphate coatings with addition Ni2+ and Mn2+ cations: Structure, corrosion resistance and paint adhesion," *Journal of Materials Research and Technology*, vol. 30, pp. 7308–7327, May 2024, doi: 10.1016/j.jmrt.2024.05.103.

[20] B. Herbáth, K. Kovács, M. Jakab, and É. Makó, "Crystal structure and properties of zinc phosphate layers on aluminum and steel alloy surfaces," *Crystals*, vol. 13, no. 3, Art. no. 369, Feb. 2023, doi: 10.3390/cryst13030369.

[21] A. H. Riyas, C. V. Geethanjali, S. Arathy, A. Anil, and S. M. A. Shibli, "Exploration and tuning of Al2O3/Mo composite for enhancement of anti-corrosion and tribological characteristics in zinc phosphate conversion coatings," *Applied Surface Science*, vol. 593, Art. no. 153370, Aug. 2022, doi: 10.1016/j.apsusc.2022.153370.

[22] X. Wu et al., "Synergistic passivation of zinc phosphate and aluminum tripolyphosphate for enhanced long-term protection of epoxy polyurethane rust-tolerant coatings," *Journal of Applied Polymer Science*, vol. 143, no. 14, Art. no. e70434, Apr. 2026, doi: 10.1002/app.70434.

[23] K. Zuo, G. Xiao, C. Du, B. Liu, Y. Li, and Y. Lu, "Controllable phases evolution and properties of zinc-phosphate/strontium-zinc-phosphate composite conversion coatings on Ti: Effect of temperature," *Surface and Coatings Technology*, vol. 447, Art. no. 128885, Oct. 2022, doi: 10.1016/j.surfcoat.2022.128885.

[24] R. M. Ramos, S. R. Kunst, L. G. Soares, E. L. Schneider, and C. T. Oliveira, "A comparison between the titanium-based and the zinc phosphate dispersion conditionings of zinc phosphate baths," *Matéria (Rio J.)*, vol. 29, no. 2, Art. no. e20240070, 2024, doi: 10.1590/1517-7076-rmat-2024-0070.

[25] S. Silva-Fernández, B. Díaz, I. Feijoo, X. R. Nóvoa, and C. Pérez, "Influence of pH and temperature in the performance of Zn phosphate conversion coatings," *Electrochimica Acta*, vol. 457, Art. no. 142510, Jul. 2023, doi: 10.1016/j.electacta.2023.142510.

[26] K. Jaioua et al., "Low-temperature zinc phosphating accelerated by triazoles for microalloyed steel in automotive cataphoresis," *Results in Engineering*, vol. 28, Art. no. 107603, Dec. 2025, doi: 10.1016/j.rineng.2025.107603.

[27] S. A. Barsana, P. Magesan, K. Jayamoorthy, and M. J. Umapathy, "Improved corrosion resistance of mild steel with poly (vinyl pyrrolidone) incorporated zinc phosphate coating," *Journal of the Taiwan Institute of Chemical Engineers*, vol. 178, Art. no. 106363, Jan. 2026, doi: 10.1016/j.jtice.2025.106363.

[28] S. R. Arunima, M. J. Deepa, L. Elias, T. R. Aju Thara, C. V. Geethanjali, and S. M. A. Shibli, "Tuning of surface characteristics of composite (WO3/BiVO4) zinc phosphate coatings for industrial applications," *Applied Surface*

Science, vol. 543, Art. no. 148822, Mar. 2021, doi: 10.1016/j.apsusc.2020.148822.

[29] X. Zhang et al., "Influence of process parameters on microstructure and corrosion properties of hopeite coating on stainless steel," *Corrosion Science*, vol. 94, pp. 428–437, May 2015, doi: 10.1016/j.corsci.2015.02.021.

[30] V. S. Kathavate, N. S. Bagal, and P. P. Deshpande, "Corrosion protection performance of nano-TiO2-containing phosphate coatings obtained by anodic electrochemical treatment," *Corrosion Reviews*, vol. 37, no. 6, pp. 565–578, Nov. 2019, doi: 10.1515/corrrev-2018-0094.

[31] M. Tamilselvi, P. Kamaraj, M. Arthanareeswari, S. Devikala, and J. A. Selvi, "Development of nano SiO2 incorporated nano zinc phosphate coatings on mild steel," *Applied Surface Science*, vol. 332, pp. 12–21, Mar. 2015, doi: 10.1016/j.apsusc.2015.01.177.

[32] A.-M. Cazac et al., "Effect of zinc, magnesium, and manganese phosphate coatings on the corrosion behaviour of steel," *Materials*, vol. 18, no. 13, Art. no. 3126, Jul. 2025, doi: 10.3390/ma18133126.

[33] A. Ayodeji, A. Eworitsemogha, D. Bamidele, and F. Ojo, "Mild steel corrosion control through locally sourced calcium oxide on zinc phosphating process," *South African Journal of Chemical Engineering*, vol. 44, pp. 147–155, Apr. 2023, doi: 10.1016/j.sajce.2023.02.001.

[34] M. Witanta, I. G. A. Arwati, and E. H. Majlan, "Natural inhibitors for corrosion protection of 6061 aluminum alloy: A review," *International Journal of Innovation in Mechanical Engineering and Advanced Materials*, vol. 7, no. 3, Art. no. 148, Oct. 2025, doi: 10.22441/ijimeam.v7i3.34713.

[35] J. Zhao et al., "Corrosion behavior of the 2024 aluminum alloy in the atmospheric environment of the South China Sea Islands," *Coatings*, vol. 14, no. 3, Art. no. 331, Mar. 2024, doi: 10.3390/coatings14030331.

[36] E. McCafferty, "Sequence of steps in the pitting of aluminum by chloride ions," *Corrosion Science*, vol. 45, no. 7, pp. 1421–1438, Jul. 2003, doi: 10.1016/S0010-938X(02)00231-7.

[37] W. Yin et al., "Revealing the atmospheric corrosion mechanism of metallic aluminum under a self-generated electric field," *Corrosion Science*, vol. 268, Art. no. 113919, Aug. 2026, doi: 10.1016/j.corsci.2026.113919.

[38] C. Jiang, G. Xiao, X. Zhang, R. Zhu, and Y. Lu, "Formation and corrosion resistance of a phosphate chemical conversion coating on medium carbon low alloy steel," *New Journal of Chemistry*, vol. 40, no. 2, pp. 1347–1353, Feb. 2016, doi: 10.1039/C5NJ02245B.

[39] X. Hao et al., "Comparative study on corrosion behaviors of ferrite-pearlite steel with dual-phase steel in the simulated bottom plate environment of cargo oil tanks," *Journal of Materials Research and Technology*, vol. 12, pp. 399–411, May 2021, doi: 10.1016/j.jmrt.2021.02.095.

[40] S. Sen, A. Chatterjee, D. Ramakanth, S. Singh, and P. K. Maji, "Recent advances in cathodic electrodeposition coatings with special reference to resin materials: A comprehensive review," *Progress in Organic Coatings*, vol. 190, Art. no. 108387, May 2024, doi: 10.1016/j.porgcoat.2024.108387.

[41] D. Saran, A. Kumar, S. Bathula, D. Klaumünzer, and K. K. Sahu, "Review on the phosphate-based conversion coatings of magnesium and its alloys," *International Journal of Minerals, Metallurgy and Materials*, vol. 29, no. 7, pp. 1435–1452, Jul. 2022, doi: 10.1007/s12613-022-2419-2.

[42] T. Duarte, Y. A. Meyer, and W. R. Osório, "The holes of Zn phosphate and hot dip galvanizing on electrochemical behaviors of multi-coatings on steel substrates," *Metals*, vol. 12, no. 5, Art. no. 863, May 2022, doi: 10.3390/met12050863.

[43] M. Eslami, V. Pachchigar, M. Sankaran, and D. V. Krogstad, "Critical influence of chemical pretreatments on the deposition and effectiveness of Zr-based conversion coating on AA2024-T3 aluminum alloy," *Applied Surface Science*, vol. 697, Art. no. 163018, Jul. 2025, doi: 10.1016/j.apsusc.2025.163018.

[44] T. D. Widodo et al., "The effect of different levels of cleanness of the pre-coat surface on adhesion and corrosion performance of A36 steel with epoxy coating," *Sinergi*, vol. 30, no. 1, Art. no. 103, Jan. 2026, doi: 10.22441/sinergi.2026.1.010.

[45] M. Doerre, L. Hibbitts, G. Patrick, and N. K. Akafuah, "Advances in automotive conversion coatings during pretreatment of the body structure: A review," *Coatings*, vol. 8, no. 11,

Art. no. 405, Nov. 2018, doi: 10.3390/coatings 8110405.

[46] C. Jiang, Z. Gao, H. Pan, and X. Cheng, "The initiation and formation of a double-layer phosphate conversion coating on steel," *Electrochemistry Communications*, vol. 114, p. 106676, May 2020, doi: 10.1016/j.elecom.2020.106676.

[47] T.-L. Nguyen, T.-C. Cheng, J.-Y. Yang, C.-J. Pan, and T.-H. Lin, "A zinc–manganese composite phosphate conversion coating for corrosion protection of AZ91D alloy: growth and characteristics," *Journal of Materials Research and Technology*, vol. 19, pp. 2965–2980, Jul. 2022, doi: 10.1016/j.jmrt.2022.06.079.

[48] M. Štulović et al., "Sustainable integrated approach to waste treatment in automotive industry: Solidification/stabilization, valorization, and techno-economic assessment," *Sustainability*, vol. 17, no. 19, Art. no. 8553, Sep. 2025, doi: 10.3390/su17198553.